Importance of cross reaction covariance data for user applications

Patrick Griffin[1*]

[1]Sandia National Laboratories, Advanced Science and Technology Division, Albuquerque, NM, USA

Abstract. The characterization of the uncertainty in radiation damage metrics presents many challenges. This paper examines the current approaches to characterizing radiation damage metrics such as hydrogen and helium gas production, material heating, trapped charge in microelectronics, and lattice displacement damage. Critical uncertainty aspects go beyond just the material cross sections and involve the consideration of energy-dependent cross reaction correlations, the recoil ion energy spectrum, and models used for the partitioning of the recoil ion energy into various forms of energy deposition. This paper starts with a review of terminology and then examines the current approaches in the characterization of uncertainty in radiation damage metrics for several applications. The major deficiencies in the uncertainty of the damage metric characterization are also identified.

1 Introduction

The nuclear data community has made great strides in improving the characterization of the uncertainty in the recommended nuclear data and in the modelling of various radiation metrics. The baseline expectation in an uncertainty characterization for an energy-dependent quantity, like a neutron cross section, includes presentation of the energy-dependent correlation matrix as well as the traditional presentation of the energy-dependent standard deviations. The challenge our community now faces is in extending our high-fidelity uncertainty characterization to derived quantities/metrics where there can be correlations between the various nuclear data inputs and models when representing the desired quantity.

This paper examines two classes of metrics where cross correlation between nuclear data quantities that describe the metric may be important in the uncertainty characterization of the metric. The first class consists of dosimetry metrics. Examples of dosimetry metrics where correlations between input terms are important include: a) neutron-induced activities in dosimeters where elemental, rather than isotopically pure, materials are used; b) gas production in materials, e.g., hydrogen and helium accumulation, bubble formation, and outgassing. The second class consists of radiation damage metrics. Example of radiation damage metrics include: a) ionizing dose and trapped charge in dielectrics found in microelectronics; b) Frenkel pair generation and evolved defects that affect carrier lifetime in semiconductors; c) material embrittlement metrics in materials, e.g., welds in iron pressure vessels used in light water reactors. A mathematical formulation for calculating a wide variety of damage metrics is introduced and examples of the importance in correlations between input terms are addressed.

2 Dosimetry metrics

Metrics used for dosimetry purposes most commonly correspond to reactions where a residual activity in an isotope is used as the relevant metric. The residual activity can be measured in different manners; emitted gammas are typically measured though the use of high purity germanium detectors (HPGe); emitted betas are typically measured using organic scintillators; hydrogen and helium generation is typically measured using atomic mass spectroscopic analysis. The following sections provide a more detailed discussion of how the covariance considerations are treated in the metrics used to represent some of these dosimetry application areas.

2.1 Activation sensors

Legacy dosimetry files, e.g., DOSDAM77 [1] and IRDF-90 [2], addressed isotopic-specific reactions of interest for dosimetry monitoring applications. However, most applications use elemental, and not isotopically enriched, activation sensors. Thus, new dosimetry libraries, e.g., IRDFF-II [3], report activation cross sections for elemental sensors. In addition, nuclear standards organizations, in standards for light water reactor dosimetry, are now referring to activities in elemental sensors, with their natural isotopic abundances, e.g., ASTM E526-22, Standard Test Method for Measuring Fast-Neutron Reaction by Radioactivation of Titanium [4].

Figure 1 shows the dosimetry cross section for the above E526 example of an elemental activation, i.e.,

* Corresponding author: pjgriff@sandia.gov

^{nat}Ti(n,X)^{46}Sc. For elemental sensors the adopted convention is to report the cross section normalized per atom of the target element. Since this ASTM standard only addresses applications for fission-based reactors, the data in this standard only goes up to 20 MeV – and only two reaction channels are relevant. However, the IRDFF-II dosimetry library uses the ENDF-6 format [5] MF10/MT5 file to report this cross section and it includes **all** relevant reaction channels up to the maximum energy in the library, 60 MeV. In this example, the IRDFF-II library entry includes cross section contributions from the following 11 channels [notated with relevant target isotopic abundance and ENDF-6 reaction identifier]:

- ^{46}Ti(n,p) {8.25%; MAT 2225, MF3/MT103}
- ^{47}Ti(n,d+pn+np) {7.44%; MAT 2228, MF10/MT5}
- ^{48}Ti(n,nd) {73.72%; MAT 2231, MF3/MT32}
- ^{48}Ti(n,2np) {73.72%; MAT 2231, MF3/MT41}
- ^{48}Ti(n,t) {73.72%; MAT 2231, MF3/MT105}
- ^{49}Ti(n,2nd) {5.41%; MAT 2234, MF3/MT11}
- ^{49}Ti(n,nt) {5.41%; MAT 2234, MF3/MT33}
- ^{49}Ti(n,3np) {5.41%; MAT 2234, MF3/MT42}
- ^{50}Ti(n,2nt) {5.18%; MAT 2237, MF3/MT154}
- ^{50}Ti(n,4np) {5.18%; MAT 2237, MF3/MT156}

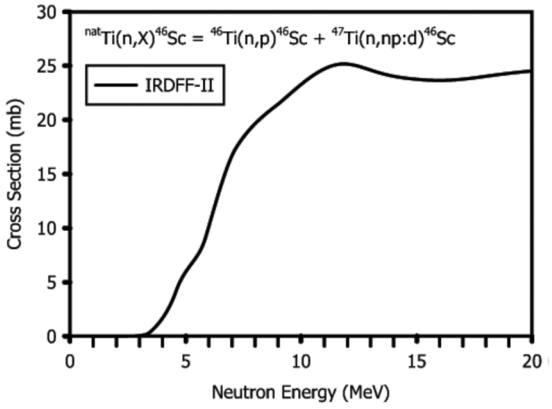

Fig. 1. ^{nat}Ti(n,X)^{46}Sc cross section (normalized per elemental Ti atom) [4]

The IRDFF-II library also includes the covariance matrix for this composite elemental activation reaction. The IRDFF-II covariance file is obtained by combining, with proper weighting, the covariance matrices for each of the individual reaction channels. The IRDFF-II covariance combination makes the assumption that the reactions are uncorrelated. However, there exists strong correlations between the separate reaction channels – and this correlation, based within the experimental data and in the model calculations, is not currently treated in generating the associated covariance matrix for the ^{nat}Ti(n,X)^{46}Sc reaction.

Many of the high threshold reactions (> 20 MeV) in the IRDFF-II library are taken from the TENDL library. The TENDL nuclear data evaluations depend heavily upon the TALYS-calculated cross sections. So, one approach to address the cross section correlation for these high threshold reaction channels, as represented in the TENDL random libraries, is to generate a covariance matrix based on a Total Monte Carlo (TMC) methodology. This approach generates a covariance matrix based upon a sampling of the underlying nuclear model data, e.g., the optical model parameters, DWBA deformations, and level density parameters, to capture the cross-reaction correlations. However, most of the IRDFF-II low energy (<20 MeV) reaction data comes from isotope-specific and reaction-specific evaluations that are produced explicitly for dosimetry applications – and which do not have associated model-based random libraries that can be sampled. One challenge in representing the uncertainty comes in how to combine the low threshold calculated covariance files, which are dominated by a consideration of the available experimental data, with the high threshold covariance files, which are determined from the parameter variation in the nuclear reaction models. A second challenge in representing the uncertainty comes from how to combine the separate isotopic-specific reaction evaluations when done for low threshold reactions, e.g., in the above example, to combine the ^{46}Ti(n,p) covariance with the ^{47}Ti(n,np) and ^{47}Ti(n,d) covariance matrices.

These three data-driven dosimetry reactions were separately derived/evaluated in the IRDFF-II evaluations, but strong correlations are expected to exist between experimental datasets used in the individual evaluations, e.g., most experiments used natural titanium samples and, as seen in Figure 2, some datapoints were taken by the same experimenters.

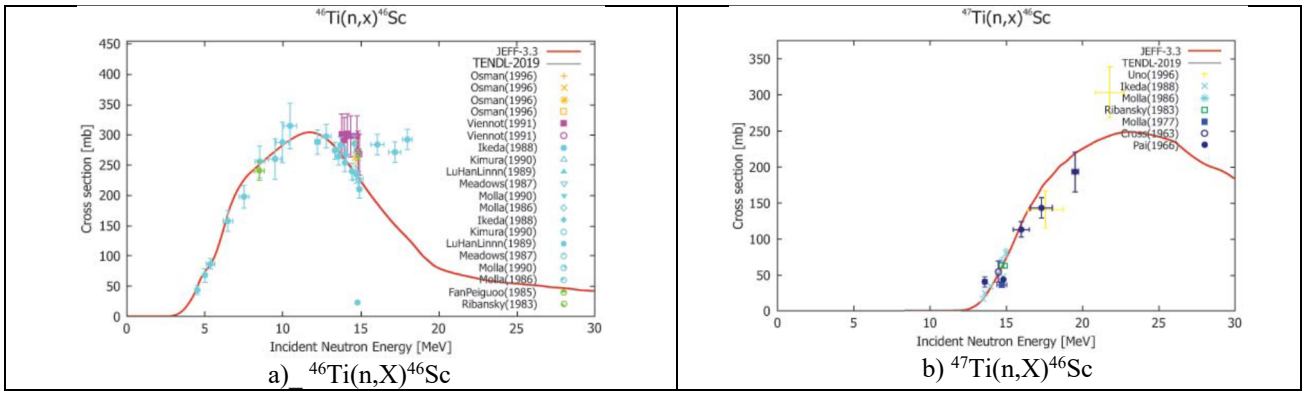

a) ^{46}Ti(n,X)^{46}Sc b) ^{47}Ti(n,X)^{46}Sc

Fig. 2. Experimental data for the ^{nat}Ti(n,X)^{46}Sc cross section from the separate titanium isotopes [4]

Cross reactions correlations can be important in addressing activation sensors, and there is room for improvement in how we address this.

2.2 Gas production

The area of gas production metrics can be divided into three categories. The first category is when the metric is used as a simple reaction identifier. An example of this category is the use of a helium accumulation fluence monitor (HAFM) as a sensor. A sample application here is found in ASTM E910 Standard Test Method for Application and Analysis of Helium Accumulation Fluence Monitors for Reactor Vessel Surveillance [6]. The covariance considerations here are nearly identical to those addressed for the activation sensors in Section 2.1. Figure 3 shows the threshold energy and cross section energy-dependence for some of the many reactions that need to be considered for helium production in elemental boron. Helium can be produced by both the ^{10}B and ^{11}B naturally occurring isotopes. Figure 4, work by A. Trkov and documented in the IRDFF-II library [3], shows that complex pathways must be considered in order to account for all the helium production mechanisms, e.g., consideration of the production of ^{8}Be and its breakup into two alpha particles. Thus, correlations in the energy-dependence of a HAFM sensor can depend upon correlations between: a) cross sections for the ^{10}B and ^{11}B naturally occurring isotopes; b) different reactions channels within a given isotope; and c) decay paths for metastable products that also produce helium, e.g., ^{10}B(n,^{3}He) → ^{3}He + ^{8}Li* → ^{3}He + 2 ^{4}He, where subsequent decay paths produce additional helium that would be totally correlated with the direct helium production from the diect reaction channel.

The second category of gas production metrics takes the various gas production reaction channels and addresses the diffusion and evolution of the generated gas as it forms voids, more complicated defects, and over-pressurized bubbles that may be subject to sudden release mechanisms, i.e., out-gassing. The normal radiation-induced lattice defects, e.g., vacancies and interstitials, can interact with released helium and affect the microstructure of evolved defects in materials such as metals or carbides. Helium-vacancy defects have been seen in helium implanted samples – and this interaction of helium with the annealing of the lattice defects results in a very complex dynamics that requires

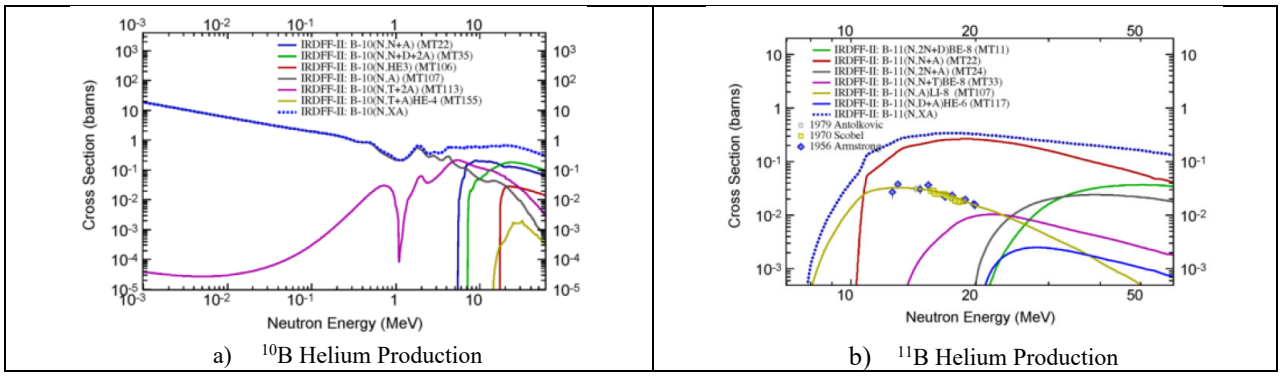

a) ^{10}B Helium Production b) ^{11}B Helium Production

Fig. 3. Helium production in the boron isotopes [3]

MT	LR	Gas	Reaction	Products	Source evaluations of IRDFF-II	
105		^{3}H	^{10}B(n,t)	→ ^{3}**H** + (^{8}Be* → 2 ^{4}He)	EAF-2010(r) ($E > 20$)	
700			^{10}B(n,t)	→ ^{3}**H** + (^{8}Be* → 2 ^{4}He)		ENDF/B-VIII.0 (
113			^{10}B(n,t2α)	→ ^{3}**H** + 2 ^{4}He	EAF-2010(r) MT105	ENDF/B-VIII.0 N
155			^{10}B(n,tα)	→ ^{3}**H** + 2 ^{4}He	EAF-2010	
106		^{3}He	^{10}B(n,^{3}He)	→ ^{3}**He** + (^{8}Li → ^{8}Be* → 2 ^{4}He)	EAF-2010	
22		^{4}He	^{10}B(n,nα)	→ n + ^{4}**He** + ^{6}Li	EAF-2010(r) ($E > 20$)	ENDF/B-VIII.0 N
32			^{10}B(n,nd)	→ n + ^{2}H + (^{8}Be* → **2** ^{4}**He**)	EAF-2010(r) ($E > 20$)	
35			^{10}B(n,nd2α)	→ n + ^{2}H + **2** ^{4}**He**	EAF-2010(r) MT32	ENDF/B-VIII.0 N
55,56,...	22		^{10}B(n,n)	→ n + ^{4}**He** + ^{6}Li		ENDF/B-VIII.0 (
55,56,...	35		^{10}B(n,n)	→ n + ^{2}H + **2** ^{4}**He**		ENDF/B-VIII.0 (
105			^{10}B(n,t)	→ ^{3}H + (^{8}Be* → **2** ^{4}**He**)	EAF-2010(r) ($E > 20$)	
700			^{10}B(n,t)	→ ^{3}H + (^{8}Be → **2** ^{4}**He**)		ENDF/B-VIII.0 (
106			^{10}B(n,^{3}He)	→ ^{3}He + (^{8}Li* →^{8}Be* → **2** ^{4}**He**)	EAF-2010	
107			^{10}B(n,α)	→ ^{4}**He** + ^{7}Li	EAF-2010(r) ($E > 20$)	ENDF/B-VIII.0 N
800			^{10}B(n,α)	→ ^{4}**He** + ^{7}Li		ENDF/B-VIII.0 (
801			^{10}B(n,α)	→ ^{4}**He** + ^{7}Li*		ENDF/B-VIII.0 (
113			^{10}B(n,t2α)	→ ^{3}H + **2** ^{4}**He**	EAF-2010(r) MT105	ENDF/B-VIII.0 N
155			^{10}B(n,tα)	→ ^{3}H + **2** ^{4}**He**	EAF-2010	

Fig. 4. Complex pathway for helium production in ^{10}B [3]

multi-scale physics models to capture the detailed behavior. In addition to this metric involving modelling of the defect evolution, the correlation between the helium release, its rate of release, and the temperature (both in the cascade where the helium is generated and in the subsequent annealing stages) are all important considerations in representing this damage metric.

The third category of gas production metrics builds upon the category two microscale description of the evolved defects and addresses the implications of the evolved gas on macroscale applications, e.g., changes in the material properties that may have implications within the application area. The realm of important correlations encompasses the correlations with the gas release rate, the application-induced temperature of the sample (as opposed to the temperature spikes due to the damage cascade), and synergies between different gasses, e.g., synergistic damage has been observed to be associated with the production of both hydrogen and helium. This synergistic effect means that empirical models for changes in material mechanical properties, due to either hydrogen or helium generation, when combined, fail to represent the observed damage when both hydrogen and helium are simultaneously introduced (this has been simulated using implantation methods).

3 Damage metrics

A discussion of the importance of correlations between different nuclear data input parameters requires us to first establish a common terminology for characterizing how these damage metrics are modelled. Section 3.1 establishes a basic framework and terminology that can represent most of the simpler damage metrics that are currently modelled and correlated with observed damage modes. The following sections look more in-depth at the correlations that can be important to a consideration of specific damage modes – and within the context of specific applications.

3.1 Terminology for calculated metrics

Common damage metrics are often modelled using easily calculated quantities such as the total kerma, displacement kerma, ionizing kerma, and displacement-per-atom (dpa). Most high-level damage metrics can be expressed as a scalar function of these quantities and can be represented as in Equation 1. This scalar metric can be modelled as a normalization factor multiplied by the convolution of the radiation field [characterized by a fluence, Φ , and a unit normalized energy-dependent spectrum, $\phi(E)$] and a response function, $\Re(E)$.

$$ {}^{facility}D_{type} = {}^{type}\mathbb{C} \bullet {}^{facility}\Phi \bullet \int_0^\infty \phi^{facility}(E) \bullet \Re_{type}(E) \bullet dE \quad (1) $$

Neutron damage is typically correlated with the details for the energy deposition in a material – and this energy deposition is related to details of the specific neutron interactions, e.g., the energy deposition, that comes from the outgoing recoil ions resulting from the neutron interaction. Because of this, most scalar response functions can be expressed, as in Equation 2, as a summation over the various reaction channels and an integration over the response due to the energy and angle of the resulting recoil particles.

$$ \Re_{type}(E) = \sum_{i,j_i} \sigma_{i,j_i}(E) \int_0^\infty dT_{R,j_i} \int_{-1}^{1} d\mu \cdot f\left(E,\mu,T_{R,j_i}\right) \cdot {}^{type-A}\Lambda\left(E_d, {}^{ion}_{type-B/D}\, T_{R,j_i}\right) \bullet {}^{type-B}\zeta\left(E_d, T_{R,j_i}, {}^{type-D}\, T_{dam}\right) \bullet {}^{type-C}\xi\left(T_{R,j_i}\right) \quad (2) $$

As described in Reference 7, in this expression: f describes the energy- and angle-dependent reaction-specific recoil spectrum; Λ , the damage partition function, describes the partitioning of energy into the relevant deposition process, e.g., ionization or displacement for some damage metrics; ζ , the threshold treatment modifier, describes the probability of Frenkel pair recombination for displacement energies near the displacement threshold energy – an angle-dependent value; and ξ , a recoil ion damage efficiency factor, describes the efficiency function relevant for a specific type of defect and typically comes from molecular dynamics code calculations. The "type-A", "type-B", "type-C", and "type-D" qualifiers that appear in the superscripts for the various terms of Equation 2 denote various conventions for those terms that have been used in the published literature. Reference 7 provides details for some examples for these designators.

Some damage metrics can be more complex than what can be captured in scalar expressions such as that shown in equations 1 and 2. One such damage metric is the linear transfer energy (LET), $\mathcal{L}$(E). The LET can be represented as in Equation 3 [8]. This type of damage metric represents a probability distribution function for charge released by a recoil ion based on its energy at the time of its creation. Rather than being characterized as a scalar quantity, it must be described as a function of a scaled response from the angle-integrated recoil spectrum, Θ , as shown in Equation 4.

$$ \mathcal{L}(E) = \sum_{i,j_i} {}^{GaAs}S\left[T_{R,j_i} \Rightarrow LET\left(\frac{A^{j_i}}{Z^{j_i}}P\right)\right] \bullet {}^{O_{i,j_i}}\Theta(T_{R,j_i}) \quad (3) $$

$$ {}^{O_{i,x}}\Theta(T_{R,i,x},E) = \sum_{i,j_i} \delta\left[j_i, O_{i,x}\right] \cdot \phi(E) \cdot \sigma_{i,j_i}(E) \cdot \int_{-1}^{1} d\mu \cdot f\left(E,\mu,T_{R,j_i}\right) \quad (4) $$

Note, Equation 3 represents the LET damage metric, a calculated metric which is an approximation for the actual damage in processes such as neutron-induced upset, where it is the actual collected charge that affects the damage in a semiconductor. This calculated damage metric neglects the change in the recoil ion LET as it down-scatters within the target lattice material and the effective electric field in a semiconductor that defines the sensitive volume over which the generated charge is collected.

This section only addresses the generic terminology for expressing the damage metrics. The details of which input quantities, as represented as in Equations 2 and 3, are correlated, and the importance of that correlation in the use of the damage metric, are addressed in later sections. This correlation between the different nuclear data input quantities, seen in Equations 2 and 3, has a significant effect on the uncertainty for the resulting damage metric. As seen in the Section 2 discussion of activation sensors, there can be a strong correlation

between reaction-channel-specific neutron cross sections within a given isotope – and between different isotopes in a naturally occurring element. What is new in the discussion of damage metrics is the correlation between additional nuclear data quantities that are addressed by the various damage-specific functions that are part of Equation 2, e.g., the recoil spectra, ion stopping power, and the damage partition function.

An additional consideration in the uncertainty characterization, based on use of the above expressions, is that the uncertainty propagation process often makes the assumption that the representation of the component-level uncertainty can be used in the form of a covariance matrix – and this often makes the assumption that the uncertainty can be represented by a normal/Gaussian distribution. This can be a significant assumption – and it is often not supported by a careful consideration of the physics behind the definition of the parameter or the sampled data. For example, when large uncertainties are present, the physical constraints of non-negativity in some quantities mean that the uncertainty often should not be described as a normal/Gaussian distribution, e.g., in the cases where a log-normal distribution or a Poisson distribution are indicated by the physical basis. If one knows the probability distribution function (pdf) associated with a parameter that influences the damage metric, it can be properly propagated through a nonlinear process into a damage metric – even if the approach is through the use of a Total Monte Carlo (TMC) sampling. Complications arise when insufficient data, or a physics-based argument, are not available to support use of the assumption that a parameter is normally distributed. Some observations on the expected probability distribution, when made at a fundamental physics-based level, can be inferred. However, when a representation of the probability distribution is made at a higher level of representation, the distribution for quantities, e.g., the Frenkel pair distribution, the ion stopping power, or the damage partition function, can be much more complicated than a normal distribution.

3.2 Nuclear data

The starting point for an investigation into the uncertainty in most radiation damage metrics, in either equation 2 or 3, is a consideration of the neutron cross section. For simplicity in this depiction/analysis, the set of reaction channels is divided into elastic, inelastic, disappearance channels (where there is no outgoing neutron in the residual channel), and "other" (reaction channels where there is an outgoing neutron in the residual channel as well as other recoil particles). This partitioning into "classes" of reactions was used because it represents the "classes" of output damage metrics automatically provided in the NJOY analysis code [9].

Using ^{28}Si as a representative case for a material of interest to the user community, in this case the semiconductor radiation damage community, Figure 5a shows the neutron energy-dependent fractional contribution from these various "classes" of reaction channels to the total kerma. Figure 5b shows the overall energy-dependent uncertainty (a 1-sigma standard deviation) in the damage energy for these various classes of reactions. In Figure 5b, in addition to depicting the various reaction "classes", the red curve shows the uncertainty for the total damage energy – as captured using a Total Monte Carlo calculation based upon sampling from the set of TENDL-2012 random evaluations. The TENDL-2012 random evaluations were used in this analysis because they were provided by the TENDL developers at the time of the initial analysis. The following discussion reflects the consistent use of these TENDL-2012 random nuclear data evaluations. These results are expected to be comparable to the results if the more recent TENDL-2015 or TENDL-2017 random files were to be used in a repeat of this analysis. The most recent TENDL library, TENDL-2021, does not provide random files for the silicon isotopes, but, a sophisticated user could use the T6 system to generate their own random libraries based on the documented TENDL-2021 input files. Figure 5 clearly shows that the total uncertainty, at high incident neutron energies (>5 MeV), is much less than the weighted sum of the uncertainty in the damage energy for the various "classes" of reactions.

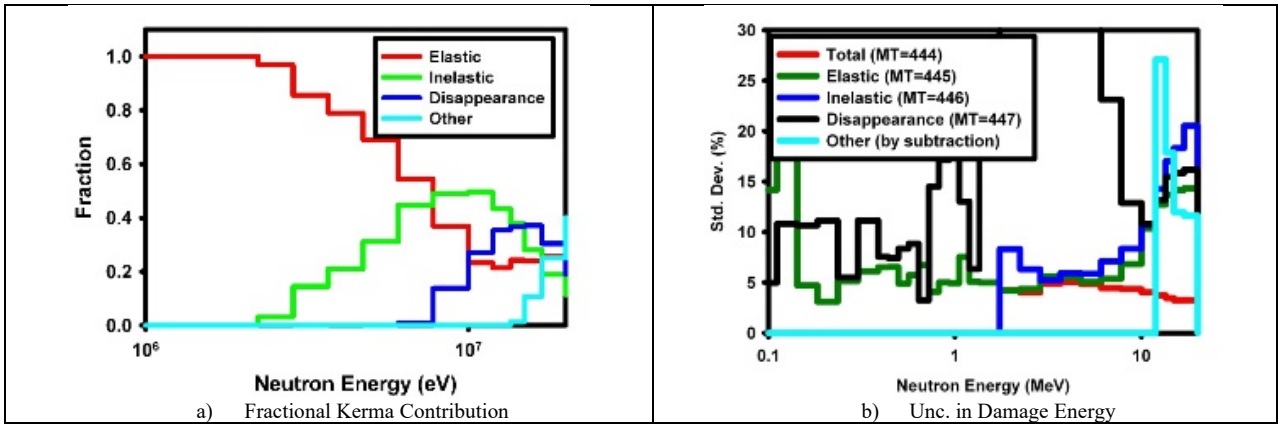

a) Fractional Kerma Contribution b) Unc. in Damage Energy

Fig. 5. Energy-dependent components of the ^{28}Si kerma (left) and the associated energy-dependent uncertainty in the damage energy (right)

This is clear evidence of the importance of including the cross-reaction covariance of different reaction channels in evaluating damage metrics.

Most current high fidelity cross section evaluations provide a good characterization of the cross-section uncertainty in the form of an energy-dependent covariance matrix in the ENDF-6 MF33/MF40 file. The covariance matrix is best considered by decomposing it into an energy-dependent standard deviation and a correlation matrix – a matrix whose entries are normalized to be between -1 and +1 and, hence, more meaningfully interpreted. Figure 6 shows how this cross-section correlation matrix for the displacement kerma can be decomposed into energy-dependent correlations for the various classes of reaction channels. Figure 6 shows that there is a very large difference in the energy-dependent correlation in these classes of reaction channels. This difference in the energy-dependent correlation underlines why a careful consideration of the covariance in the various reaction channels must be included in the derivation of the uncertainty of radiation damage metrics.

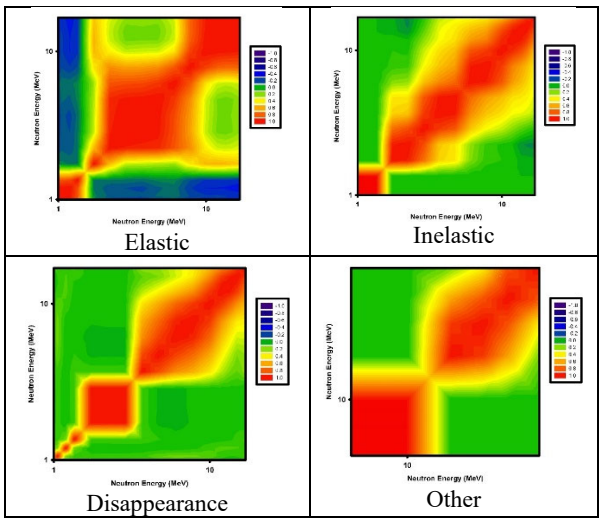

Fig. 6. Correlation matrices in the ^{28}Si displacement kerma for various classes of reactions

In order to provide a context for the importance of addressing the energy-dependent and cross-reaction correlation, one must look at the damage metric relative to a given neutron spectrum. As a representative case, we looked at the uncertainty in the ^{28}Si total kerma, ionizing kerma and displacement kerma when a material is exposed to the ^{252}Cf spontaneous fission neutron spectrum, notated as ^{252}Cf(s.f.). Table 1 shows the resulting uncertainty in the damage metrics due only to the nuclear data, i.e., the cross sections, when treated in a properly correlated manner using the Total Monte Carlo approach, versus when the various "classes" of reaction channels are treated as fully correlated (in energy) and summed, i.e., the case where the proper energy-dependent correlation is not taken into account and a proper correlation matrix is replaced by a correlation matrix where all entries are unity (this case represents consideration of the energy-dependent standard deviations, but not the energy-dependent correlations). A factor of two difference is seen in the resulting spectrum-averaged uncertainty for both damage metrics in this neutron field. A similar analysis, shows that cross-reaction correlations are also important for the damage metrics [14].

Table 1. Uncertainty contributions from the nuclear data for ^{28}Si damage metrics in the ^{252}Cf(s.f.) neutron field.

Metric	Fully Energy Correlated	Properly Correlated
Total Kerma	6.283%	3.817%
Ionizing Kerma	7.299%	4.946%
Displacement Kerma	4.815%	2.653%

3.3 Recoil spectra

After the cross section, the next most important quantity in assessing the uncertainty in damage metrics in either equation 2 or 3, is a consideration of the neutron-induced residual atom recoil spectra. The need here goes beyond a desire to evaluate the importance of cross reaction recoil spectra. The current ENDF-6 format [5] does not even support capturing the uncertainty in the recoil atom spectra.

In the absence of a nuclear data format that addresses the uncertainty in the recoil spectra, the only available approach to shed light on this uncertainty is to compare the recoil spectra from different evaluations. Figure 7a compares the elastic recoil spectra for 10 MeV incident neutrons on ^{28}Si for four modern nuclear data evaluations. For elastic scattering, the kinematics totally control the recoil spectrum and the observed variation is due to differences in the angular distribution. Figure 7b shows the variation in the ENDF/B-VII angular distribution as a function of neutron energy.

For transmutation reactions, there can be a very large variation in the recoil atom spectrum – especially near the reaction threshold energy. Figure 8 shows the large variation seen in the shape of the primary recoil atom spectra. As is seen in Fig. 8b for the (n,2n) reaction at 17.8 MeV incident neutron energy, this difference in recoil spectrum results is a factor of two difference in the resulting ion recoil energy that goes into the creation of Frenkel pairs. The ENDF/B-VII recoil spectrum came from GNASH code calculations, while the TENDL-2012 recoil spectra come from TALYS code calculations. Future analysis needs to look at the independence between the modelling of the recoil atom spectra for transmutation reaction channels in various Hauser-Feshbach codes such as GNASH, TALYS, EMPIRE, CCONE, and CoH3. Is there a strong correlation between computational models in the different codes? When Total Monte Carlo analysis is done by varying the nuclear data parameters, e.g., as guided by the uncertainty in the RIPL-3 database, is the variation in the model parameters sufficient to capture the degrees of freedom in the underlying physics that controls the reaction processes? Significant work remains to be done in understanding the influence of uncertainty and correlations in the recoil spectrum on the damage metrics used by the various applications.

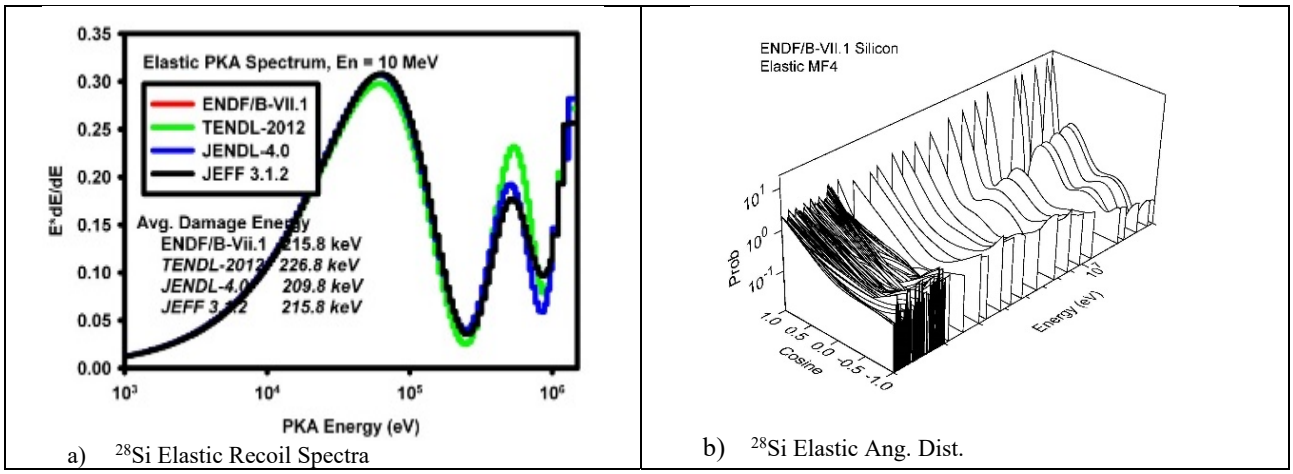

a) ^{28}Si Elastic Recoil Spectra b) ^{28}Si Elastic Ang. Dist.

Fig. 7. ^{28}Si elastic scattering

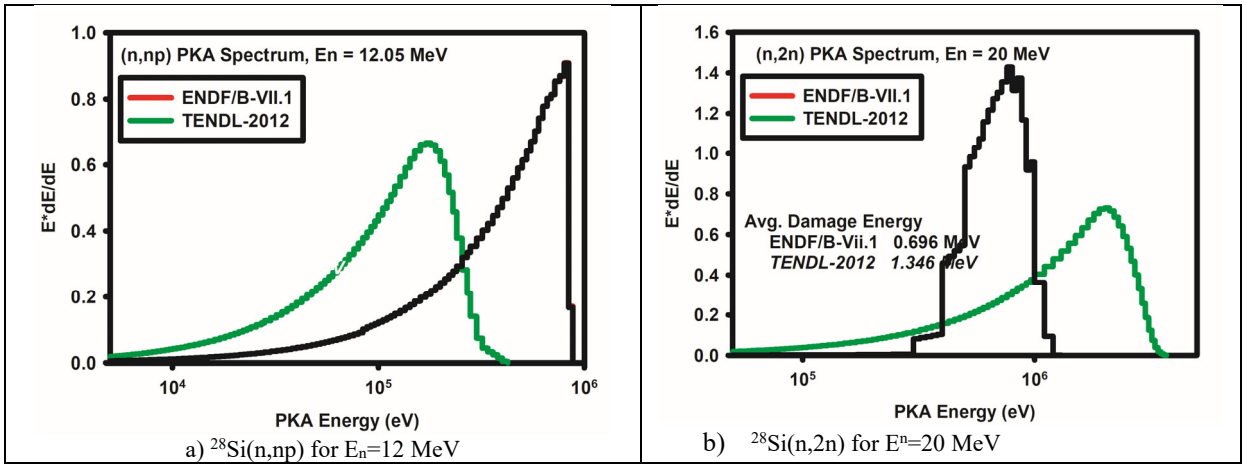

a) ^{28}Si(n,np) for E_n=12 MeV b) ^{28}Si(n,2n) for E^n=20 MeV

Fig. 8. ^{28}Si primary recoil atom spectra from transmutation reaction channels

3.4 Stopping power

After the uncertainty in the recoil spectrum has been addressed, attention then goes to how the energy from the recoil atoms is deposited in a material. This energy deposition is given by the stopping power for an ion in a material – and the stopping power can be divided into an electronic (ionizing) and a nuclear (lattice displacement, including lattice phonon generation) component.

The stopping power in silicon is depicted in Figure 9 [10]. The symbols represent experimental datapoints and the curve represent model-based calculations. Interatomic potentials are usually calibrated to measurements, including the stopping power data. Figure 10a shows the variation that can result in the damage partition function, the division of the stopping power into ionization and displacement, when integrated along the ion slowing down trajectory, into the total fraction of the energy that goes into displacements rather than into electron production. This figure shows the difference that results from use of the Akkerman damage partition function, which uses the Ziegler, Biersack, and Littmark (ZBL) potential [11], versus the Robinson partition function [12], that uses the Lindhard, Scharff, and Schiott (LSS) approach with the Thomas-Fermi screening function over the Coulomb potential and the Firsov non-local free uniform gas model for the inelastic energy loss.

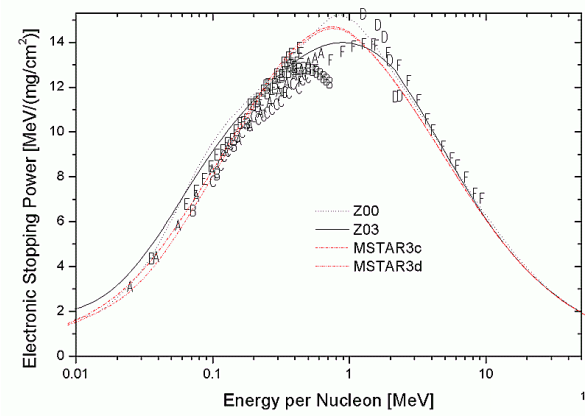

Fig. 9. Silicon stopping power [10]

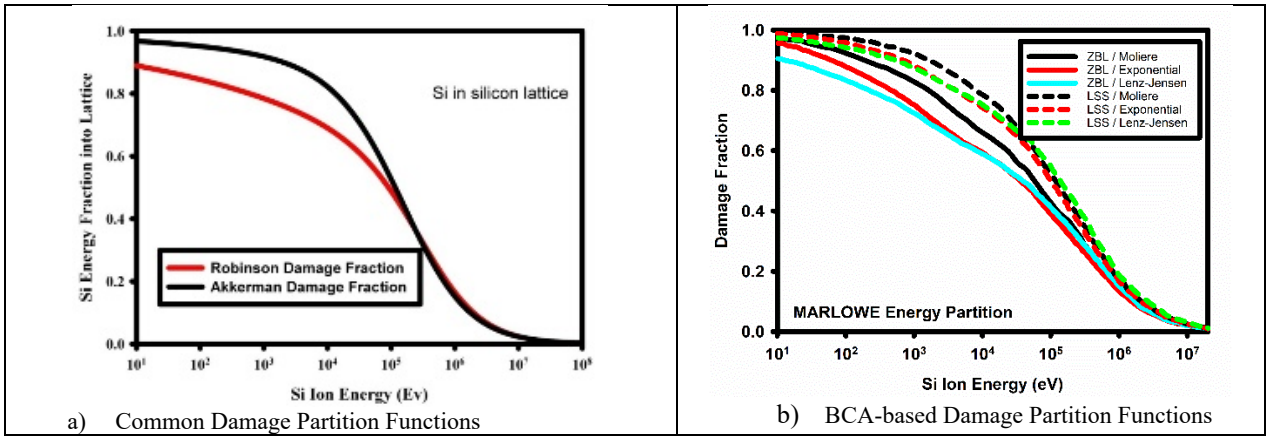

Fig. 10. Variation in the silicon partition function [13]

Figure 10b shows the variation in the damage partition function that can result when binary collision approximation (BCA) theory codes are used, with a range of interatomic potentials, to capture this division of deposited energy.

4 Application to the behavior of semiconductors

Section 3 addressed the various uncertainty contributors that affect damage metrics that are sensitive to the details of the energy deposited by a neutron interaction. The Section 4 focus is on the application area of electronics damage to semiconductors and examines three generic categories of damage: a) permanent damage; b) single event effects; and c) stochastic effects in small feature size microelectronics.

4.1 Permanent neutron damage metrics

To place this in context, we consider a representative application – permanent neutron radiation damage to silicon semiconductors. If we look at the semiconductor minority carrier recombination lifetime, the damage metric that represents the change in gain of a bipolar transistor, the calculated metric is the damage energy, i.e., the energy that goes into the creation of primary Frenkel pair defects. Figure 11 shows the correlation matrices for the various uncertainty contributors to the silicon damage energy, i.e., nuclear cross section data, interaction potentials for the recoil ion energy deposition, and close Frenkel pair recombination aspects for threshold displacement energies near the lattice binding energy. Each of these uncertainty contributors has a different energy-dependent weighting and a different correlation matrix. These three different contributors have a different physics basis and, within the modelling approach, can be considered to be uncorrelated. The bottom-right plot in Figure 11 shows the resulting total correlation matrix for the composite effect. The strong energy-dependent correlation clearly shows that this correlation in the energy-dependent response must be taken into account when using modelling to predict radiation damage that occurs in real-world applications.

The strong energy-dependent correlation seen in Figure 11, especially for the uncertainty due to the interaction potential, shows why application-specific metrics often use a normalized damage metric to compare neutron irradiation in different environments, e.g., the use of the 1-MeV equivalent fluence for radiation damage to silicon or GaAs electronics. When a normalization constraint is applied, there can be a very large decrease in the resulting uncertainty when comparing damage between different radiation environments. For other applications, such as embrittlement of the pressure vessel in pressurized water reactors (PWR), an effective normalization takes place by constraining the application of the metric to a narrow range of irradiation conditions and applying a damage metric that addresses correlations due to material impurities.

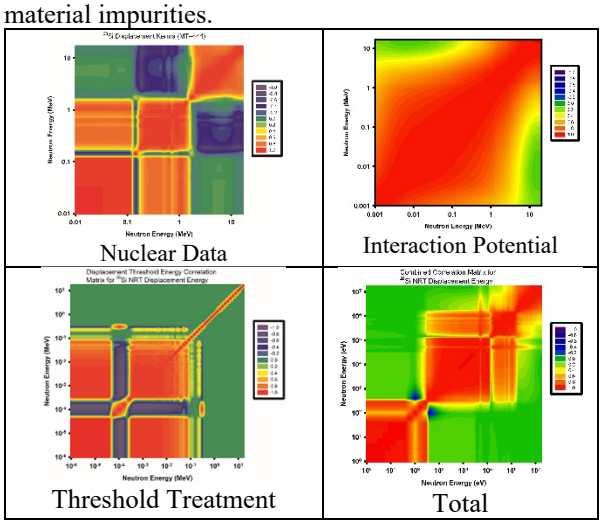

Fig. 11. Correlation matrices various uncertainty contributors in the ^{28}Si damage energy [7]

4.2 nSEEs

Neutron single event effects (nSEE) is a category of neutron damage where the physics behind the damage is related to the charge generated within a "sensitive volume" due to a single neutron interaction and collected within the clock cycle for the device operation. Since the device-specific charge collection volume can have a complex geometry, a geometry that is affected by changes in the local electric field resulting from a high

energy ion moving through the volume, the more accurate charge collection metric of collected charge is often replaced through the use of the threshold value for the LET of the recoil ion. Since the recoil ion can have a range of energies, based on the stochastic consideration of the neutron interaction (the type of reaction and the angular distribution for reaction products), the commonly used damage metric is the pdf for the LET, as seen in Equation 3.

Figure 12a shows the LET pdf for a 14 MeV neutron and for the Annular Core Research Reactor (ACRR), a pool-type fission reactor. Figure 12b shows the cumulative probability distribution (cdf) for these same neutron spectra. Since the damage state is related to the probability of the LET being above a given threshold value, the cdf is the useful damage metric.

Since the damage is related to the probability of a neutron interaction resulting in a recoil ion with an LET above a threshold value, and since the same recoil ion LET can be generated from different incident neutron energies, the interpretation of the uncertainty analysis dependents upon both the neutron spectrum and the response function. The uncertainty in the LET response relates back to the uncertainty in the both the recoil atom energies and in the ion stopping powers. Figure 13a shows this correlation in the LET distribution when a device is exposed to the ACRR free field neutron environment. Figure 13b compares the energy-dependent standard deviations in the pdf and cdf for both the ACRR and the ^{252}Cf(s.f.) neutron environments. Both the pdf and cdf are seen to have a similar standard deviation in these neutron spectra. The difference in the magnitude of the standard deviations between the two spectra is due to the uncertainty in the underlying neutron spectrum characterization, i.e., the ^{252}Cf(s.f.) neutron spectrum is much better characterized.

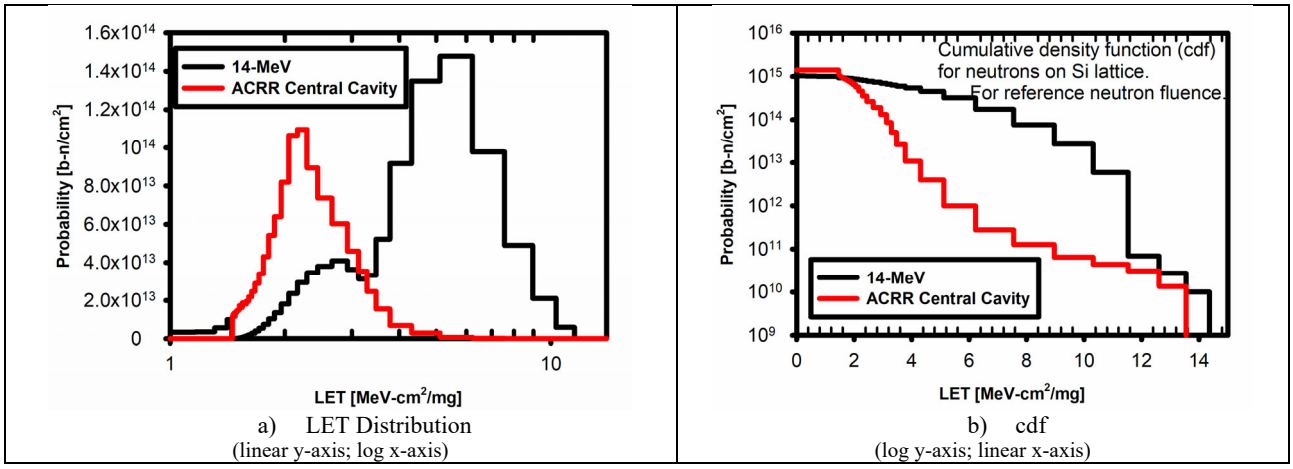

a) LET Distribution (linear y-axis; log x-axis)

b) cdf (log y-axis; linear x-axis)

Fig. 12. Silicon LET distribution for two neutron spectra [8]

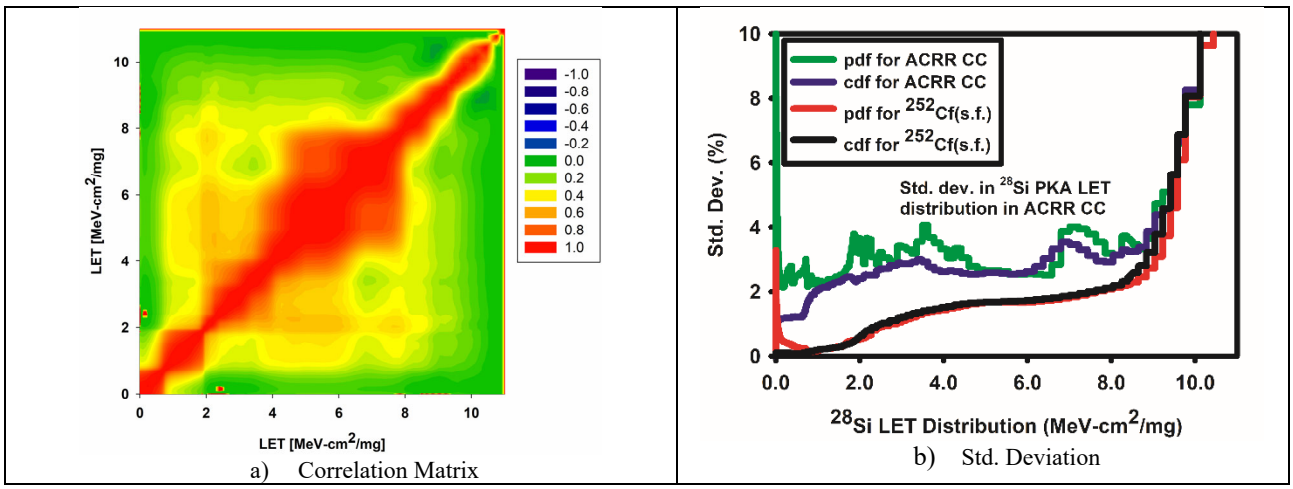

a) Correlation Matrix

b) Std. Deviation

Fig. 13. Uncertainty in the cdf for silicon LET in a pool-type reactor spectrum and in ^{252}Cf(s.f.) spectrum [8]

4.3 Stochastic considerations

As the state-of-the-art in silicon electronics goes towards the use of smaller feature sizes (<12 nm), when the damage mechanism depends upon energy deposition within a sensitive device volume, the traditional use of calculated damage metrics is no longer sufficient. When the number of neutron-induced interactions within the sensitive volume is a few rather than hundreds, the use of average damage metrics, such as an average number of Frenkel pairs, an average damage energy or an average kerma becomes less applicable. Now the stochastic variation in the damage must be considered.

Figure 14a shows the pdf for the number of Frenkel pairs generated due to an incident 100-keV silicon ion on a silicon lattice. This figure plots the results of simulating 897 cascades. The total number of Frenkel pairs generated in the cascade is depicted on the x-axis

and the frequency of this occurrence is plotted on the y-axis. This 100-keV silicon ion in a silicon lattice results in an average of 680 Frenkel pairs with a pdf having a full-width-at-half-maximum (FWHM) of 129. While this pdf can be considered to approximate a Gaussian distribution, it does have a low tail in the distribution. Figure 14b shows the results for a 1 MeV neutron, which samples over a range of neutron reaction channels and the resulting recoil atom energies. This case results in an average of 244 Frenkel pairs with a FWHM of 216. This is a very non-Gaussian distribution. The source of the shape in this distribution is traced directly back to the distribution of recoil ion energies from a 1 MeV neutron interaction, i.e., a 1 MeV neutron has an average recoil ion energy of 38-keV but with a FWHM of 31 keV for the recoil energy.

Modern electronic circuits often employ a balancing of transistors in the front-end electronics in order to extend the applicable operation range of the circuit. When these devices have a small feature size, the use of calculated damage metrics based on average interactions may no longer be justified. For example, consider an operational amplifier design where the front-end transistors typically incorporate this type of design and the applicable performance metrics are offset voltage, input bias current, and slew rate. These circuit-level performance metrics are calculated from the device-level displacement damage and charge release metrics. In order to properly predict the reliable operation of these devices in radiation, the stochastic level variation in the device-level damage metrics must be sampled – and this sampling must take into account the non-Gaussian nature of the damage distributions. Use of damage metrics based on an "average" neutron interaction is no longer sufficient. While the initial neutron interactions in the different frontend electronic devices can be considered to be uncorrelated, the correlations in the underlying damage mechanisms must be applied to the pdfs such as that shown in Figure 14b.

5 Conclusion

Th importance of correlations in modelling the uncertainty in radiation damage metrics is shown to be very dependent upon the application. This paper outlined a mathematical formulation that can be applied to most currently used device-level radiation damage metrics. Some uncertainty contributions are strongly correlated, e.g., different reaction channels, and should always be treated with high fidelity. High fidelity modelling can be a challenge – and one must often use a TMC approach in order to capture the critical correlations. Other uncertainty contributions can, based on physics considerations, be considered to be uncorrelated and are more easily treated, e.g., for permanent neutron damage modes, the uncertainty in the neutron spectrum is generally uncorrelated with the uncertainty in the response metric. An exception is addressed here for some damage metrics, such as nSEE, where the relevant physics depends upon the distribution of recoils and the damage is parametrized in terms of a distribution and a threshold vulnerability value.

Results of a careful treatment of correlations between uncertainty contributors were summarized for a range of damage modes in modern electronics. Some deficiencies in current treatment were identified, e.g., a calculated damage metric is based upon a Frenkel pair generation whereas observed damage is based upon evolved defects. For emerging small feature-size electronics, the importance of the stochastic variation in the neutron radiation damage was highlighted – exposing a deficiency in our use of average damage metrics.

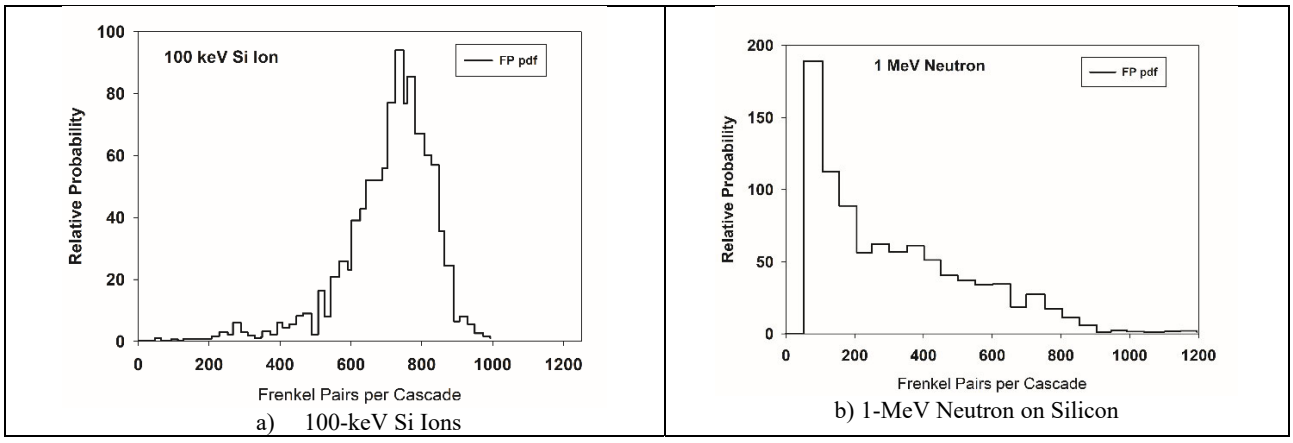

a) 100-keV Si Ions b) 1-MeV Neutron on Silicon

Fig. 14. Probability distributions for the number of Frenkel pairs created

Acknowledgement

The author wished to acknowledge the IAEA for their leadership in organizing the CRP that focused the international contributions that led to the development of the IRDFF-II library and for the separate technical contributions their staff made to the library contents. Many examples of that effort are cited in this paper as examples of the importance of addressing correlations in metrics.

This work was supported in part by the U.S. Department of Energy under contract DE-NA0003525. Sandia National Laboratories is a multi-mission laboratory managed and operated by National Technology and Engineering Solutions of Sandia, LLC, a wholly owned subsidiary of Honeywell International, Inc., for the U.S. Department of Energy's

National Nuclear Security Administration under contract DE-NA0003525.

The views expressed in the paper do not necessarily represent the views of the U.S. Department of Energy or the United States Government.

References

1. W. L. Zijp, K. H. Appelman, H. J. Nolthenius, and H. CH. Rieffe, *Damage Cross Section Library (DAMSIG77)*, report **ECN-36** (Feb. 1978).
2. N.P. Kocherov, P.K. McLaughlin, *The International Reactor Dosimetry File (IRDF-90, Version 2)*, Report **IAEA-NDS-141**, Rev. 2, International Atomic Energy Agency, (Oct. 1992).
3. A. Trkov, P.J. Griffin, et al., "IRDFF-II: A New Neutron Metrology Library", Nuclear Data Sheets, **163**, 1-108 (2020).
4. ASTM E526-22, Standard Test Method for Measuring Fast-Neutron Reaction by Radioactivation of Titanium, ASTM International, West Conshohocken, PA (2022)
5. A. Trkov, M. Herman and D. A. Brown (Eds.), *ENDF-6 Formats Manual*, CSEWG Document **ENDF-102**, Report **BNL-203218-2018-INRE**, Brookhaven National Laboratory, Upton, NY (2018) https://www.osti.gov/biblio/1425114/
6. ASTM E910, Standard Test Method for Application and Analysis of Helium Accumulation Fluence Monitors for Reactor Vessel Surveillance, ASTM International, West Conshohocken, PA (2022)
7. P.J. Griffin "Uncertainty characterization of silicon damage metrics", IEEE Trans. Nucl. Sci., **66**, pp. 327-336 (2019)
8. P.J. Griffin, A.J. Konig, D. Rochman, "Impact of Nuclear Data Uncertainty in the Modelling of Neutron-Induced Recoil Atom Energy Distributions in Silicon", IEEE Trans. Nucl. Sci., **66**, pp. 1719-1729 (2019)
9. R.E. MacFarlane, D.W. Muir, R.M. Boicourt, A.C. Kahler, J.L. Conlin, W. Haeck, *The NJOY nuclear data processing system, version 2016*, Los Alamos National Laboratory, report **LA-UR-17-20093** (2016) https://github.com/njoy/
10. H. Paul, *Stopping Power of Matter for Ions: Graphs Data Comments and Programs*, (Sep. 2018) Available: https://www-nds.iaea.org/stopping/stopping_heav.html.
11. J. F. Ziegler, J. P. Biersack and U. Littmark, *The Stopping and Range of Ions in Solids*, Pergamon Press, Inc., New York (1985) https://link.springer.com/chapter/10.1007/978-3-642-68779-2_5
12. M. T. Robinson, *Nuclear Fusion Reactors, Nuclear Fusion Reactors*, Proceedings of a conference held at UKAEA Culham Laboratory, Abingdon, 17-19 Sept. 1969, British Nuclear Energy Soc., pp. 364-378 (1970) https://www.icevirtuallibrary.com/doi/abs/10.1680/nfr.44661.0025.
13. P.J. Griffin, P.J. Cooper "Influence of the Damage Partition Function on the Uncertainty of the Silicon Displacement Damage Metric", IEEE Trans. Nucl. Sci., **64**, pp. 574-581 (2016)
14. Nuclear Reaction Data and Uncertainties for Radiation Damage, IAEA report INDC(NDS)-0719, August, 2016. https://www-nds.iaea.org/publications/indc/indc-nds-0719.pdf